Synthesis of Octopus-Tentacle-Like Cu Nanowire-Ag Nanocrystals Heterostructures and Their Enhanced Electrocatalytic Performance for Oxygen Reduction Reaction

Min Han,[†,‡] Suli Liu,[†] Linyan Zhang,[†] Can Zhang,[†] Wenwen Tu,[†] Zhihui Dai,*[,†] and Jianchun Bao*[,†]
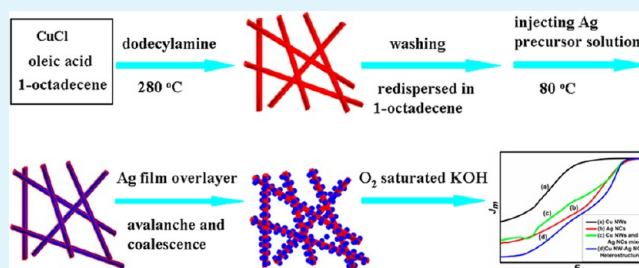
[†]Jiangsu Key Laboratory of Biofunctional Materials, School of Chemistry and Materials Science, Nanjing Normal University, Nanjing 210097, P. R. China

[‡]State Key Laboratory of Coordination Chemistry, School of Chemistry and Chemical Engineering, Nanjing National Laboratory of Solid State Microstructures, Nanjing University, Nanjing 210093, P. R. China

S Supporting Information

ABSTRACT: In this article, the novel octopus-tentacle-like Cu nanowire-Ag nanocrystals heterostructures have been fabricated in solution phase via heterogeneous nucleation and growth of Ag nanocrystals on presynthesized Cu nanowires. The growth environment and dynamic factors of Ag nanocrystals play an important role for formation of such heterostructures. Combined the physical constants of Cu and Ag with a series of control experiments, the epitaxial growth means of Ag nanocrystals on Cu nanowire is found to abide by "layer-plus-island" (Stranski-Krastanow) mode. Because of the presence of multiple junctions and strong synergistic effect of their constituents, the obtained heterostructures exhibit greatly enhanced electrocatalytic performance toward oxygen reduction reaction compared with that of pure Ag nanocrystals, Cu nanowires, and mechanically mixed dual components as well as recently reported some non-Pt materials, which can be served as an alternative cathodic electrocatalyst to apply in alkaline fuel cells. Moreover, our method can be extended to fabricate octopus-tentacle-like Cu nanowire-Au nanocrystals and Cu nanowire-Pd nanocrystals heterostructures.

KEYWORDS: Cu nanowires, Ag nanocrystals, heterostructure, heterogeneous nucleation and growth, electrocatalysis, oxygen reduction reaction

1. INTRODUCTION

Metal heteronanostructures have received great interest because of not only their multifunctional properties but also the new features arising from the electronic coupling of different components, which endow them a wide variety of promising applications in plasmonics, catalysis, gas storage, and actuator.[1−10] Many methods, including electrochemical deposition,[11,12] gas-induced surface segregation,[13] seed-mediated epitaxial growth,[14−16] self-assembly,[17] one-pot reduction or thermal decomposition,[18,19] spray pyrolysis,[20] and so on, have been developed to synthesize desired metal heterostructures. Among those methods, seed-mediated growth has been proved to be an efficient avenue to fabricate concentric core−shell type[21−26] and pearlike or cloverlike binary noble metal nanocrystals (NCs)[27] as well as multisegmental metal nanorods.[28] The mostly used "seeds" are polyhedral noble metal NCs. As an important building block, the metal nanowires (NWs) are seldom used as "seeds" to epitaxially grow another metal. To the best of our knowledge, only Au[29] and Pd[30] NWs have been used as "seeds" to grow Pt nanodendrites on their surfaces. The cheap metal NWs (e.g. Cu), which possess excellent electronic transport and catalytic properties, have not been effectively used as a platform for integrating noble metal

NCs (e.g., Ag) to fabricate novel "1D-0D" type (e.g., octopus-tentacle-like) heteronanostructures. In such heterostructural configuration, several advantages can be expected: (i) the noble metal NCs can be fully exposed and maximally utilized, beneficial to reduce the cost; (ii) the cheap metal NWs not only provide the opportunity to create multiple junctions but also promote the electronic transfer process; (iii) the effective electronic coupling between cheap and noble metals may enhance their catalytic performance. However, because of large lattice mismatch (e.g., 13% for Cu and Ag) and complicated reaction environment, synthesis of such heterostructural configuration in solution phase is a challenge issue in current chemistry and material science.

Improving the sluggish kinetics of cathodic oxygen reduction reaction (ORR) is critical to advancing the hydrogen fuel cell technology.[31,32] For this purpose, it is necessary to design highly active and long durability electrocatalysts. In the past several years, substantial research efforts have been paid on geometric structure or support selection of Pt[33−38] and Pt-
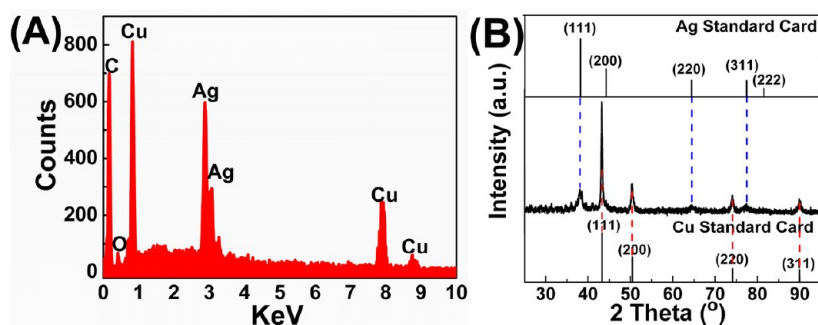
Figure 1. (A) EDS and (B) XRD patterns of the octopus-tentacle-like Cu NW-Ag NCs heterostructures.

based bimetallic NCs[39−43] to meet those challenges. Recently, in order to reduce cost and promote application of fuel cell, exploring and synthesizing non-Pt electrocatalysts for ORR have attracted many researchers' interests. For example, some Pd-based bimetallic NCs,[44−47] late transition metal chalcogenide NCs,[48] N-doped carbon nanostructures,[49] graphene supported Co_3O_4 NCs,[50] and $M_xMn_{3-x}O_4$ (M = divalent metals) NCs[51] have been found to possess excellent electrocatalytic activity for ORR in acidic or alkaline media. As one of the important noble metals, Ag is cheaper than that of Pt and Pd, which can catalyze ORR in alkaline media.[52,53] Inspired from Pt- and Pd-based bimetallic electrocatalysts, incorporating other metal into Ag lattice to form alloy or growth of Ag "skin" on other metal surface to generate heterostructure may be a feasible strategy to enhance catalytic performance of Ag for ORR due to effective electronic structure mediation of Ag by alloying or hybridization with other metal. Up to now, some Ag-based alloy or heterostructures have been employed to catalyze ORR.[54−59] However, there is nearly no report on the study of ORR by using Ag−Cu bimetallic system. Considering that metal nanowire or free-standing nanowire membrane can improve both the activity and stability of ORR electrocatalysts,[33−36] we are interested in integrating Ag NCs on cheap metal (e.g., Cu) nanowires to fabricate novel heterostructural electrocatalyst for ORR.

Here, we report the synthesis of octopus-tentacle-like Cu NW-Ag NCs heterostructures and their electrocatalytic performance for ORR. To fabricate the heterostructures, Cu NWs with the diameters of about 16−32 nm (see Figure S1 in the Supporting Information) are first prepared via a modified method of Han and coauthors,[60] i.e. thermal treatment of CuCl in the presence of oleic acid (OA), dodecylamine (DDA) and 1-octadecene (ODE). After washing for several times, the obtained Cu NWs are dried in vacuum and then used as seeds to grow Ag NCs. The growth environment and dynamic factors, such as the type and concentration of surfactants, the amount of Ag precursors and reaction temperature, are found to affect the formation of high quality octopus-tentacle-like Cu NW-Ag NCs heterostructures. Combined the physical constants of Cu and Ag with a series of control experiments, the epitaxial growth means of Ag NCs on Cu NW is discussed. Furthermore, the obtained heterostructures exhibit greatly enhanced electrocatalytic activity toward ORR compared with that of pure Ag NCs, pure Cu NWs, and mechanically mixed dual components as well as some reported non-Pt electrocatalysts, showing great promise to apply in alkaline fuel cells with the advantage of low cost and high mass current density.

2. EXPERIMENTAL SECTION

2.1. Synthesis of Cu NW-Ag NCs Heterostructures. In a typical synthesis, 6.4 mg of Cu NWs solid (about 0.1 mmol) was mixed with 5 mL of ODE in a 50 mL three-neck flask. Then, the reactor was heated to 80 ° C in an oil bath with continuous magnetic stirring. After 30 min, Ag precursor solution obtained by dissolving 0.2 mmol of $AgNO_3$ in 0.5 mL of OA, 0.5 mL of DDA, and 5 mL of ODE at 50 °C, was quickly injected into the reaction system. When reacting at 80 °C for 6 h, the reactor was naturally cooled down to room temperature. Ten mL of heptane and 5 mL of absolute ethanol were added and the crude product was separated by centrifugation at 10000 rpm for several minutes. The obtained crude product was washed by heptane and absolute ethanol for 3 times to remove the byproducts. Finally, the product was dried and stored in vacuum.

2.2. Material Characterization. The X-ray energy-dispersive spectra (EDS) were taken on a JSM-5610LV-Vantage typed energy spectrometer. The powder X-ray diffraction (XRD) patterns were recorded on a D/max 2500VL/PC diffractometer (Japan) equipped with graphite monochromatized Cu Kα radiation (λ = 1.54060 Å). Corresponding work voltage and current is 40 kV and 100 mA, respectively. MDI Jade 5.0 software was used to deal with the acquired diffraction data. The transmission electron microscopy (TEM) images were taken on a JEM-200CX instrument (Japan), using an accelerating voltage of 200 kV. High-Resolution transmission electron microscopy (HRTEM) images were obtained on JEOL-2100F apparatus at an accelerating voltage of 200 kV. The UV−vis absorbance spectra were taken on Cary 5000 UV−vis−NIR spectrophotometer.

2.3. Fabrication of Modified Glassy Carbon Disk Electrodes (GCEs). Before the electrocatalytic experiments, the obtained Cu NW-Ag NCs heterostructures were dispersed into 10 mL heptane to obtain a suspension. The concentration of the suspension was about 1 mg mL^{-1}. The GCEs (5.0 mm in diameter) were first polished with alumina slurries (0.3 and 0.05 μm) and then cleaned by sonication in 0.1 M HNO_3, H_2SO_4 and nanopure water for 10 min successively. Twenty-five microliters of the prepared heterostructure suspension was then dropcast onto the clean GCE surface by a microliter syringe. After drying at a gentle N_2 stream for about 20 min, 15 μL of 1% Nafion solution was dropped on the electrode surface and dried in a N_2 stream. Thus, the Cu NW-Ag NCs heterostructure modified GCEs were fabricated. For comparison, the pure Cu NWs and pure Ag NCs modified GCEs as well as the mechanically mixed Cu NWs and Ag NC sample modified GCE were also prepared using the same procedure.

2.4. Electrocatalytic Measurements. The electrocatalytic performances of various modified GCEs were tested in electrochemical cell with a three-electrode configuration. A Pt wire and an Ag-AgCl electrode were used as an auxiliary and reference electrodes, respectively. GCEs covered with Cu NW-Ag NCs heterostructures, pure Cu NWs and pure Ag NCs as well as the mechanical mixtures of Cu NWs and Ag NCs were used as the working electrodes. Rotating disk voltammetry was performed on Gamry's Rotating Disk Electrode (RDE710) at a rotating rate of 1600 rpm. O_2 reduction reactions were examined by first bubbling the electrolyte solution (0.1 M KOH) with high purity O_2 for 20 min and then blanketing the solution with an O_2 atmosphere during the entire experimental procedure. All electro-

6655

dx.doi.org/10.1021/am301814y | ACS Appl. Mater. Interfaces 2012, 4, 6654−6660

chemical experiments were carried out with a CHI 660C electro-chemistry workstation (Shanghai Chenhua Instrument Factory, China) at room temperature.

3. RESULTS AND DISCUSSION

Figure 1 shows the EDS and XRD patterns of the Cu NW-Ag NCs heterostructures. From the EDS pattern (Figure 1A), we can see that the main elements in the obtained sample are Cu and Ag. The detected C and O elements originate from the surface capping reagents or adsorbed air. Further information on the components, crystallinity and phase structure of the sample comes from the XRD analysis (Figure 1B). In the $25° < 2\theta < 95°$ range, seven obvious and sharp diffraction peaks can be observed, indicating that the obtained product is well crystallined. The four diffraction peaks shown by the red dashed lines are assigned to (111), (200), (220), and (311) planes of face-centered cubic (fcc) phase Cu (JCPDS-03−1005). While the other three peaks indicated by the blue dashed lines can be indexed to (111), (220), and (311) planes of fcc phase Ag (JCPDS-04−783). According to Scherrer formula, the average grain sizes for Cu and Ag in the sample are calculated to be about 19.8 and 10.4 nm, respectively. Compared with the standard cards for Cu and Ag, the position of the diffraction peaks in the obtained product do not show shift, implying that the Cu NWs "seeds" and deposited Ag NCs are phase segregated, not alloyed. That is to say, the obtained products are heterostructures, which can be further confirmed by TEM and HRTEM as well as EDS mapping analysis.

Figure 2 gives the TEM and HRTEM images of the obtained Cu NW-Ag NCs heterostructures. From the low magnification
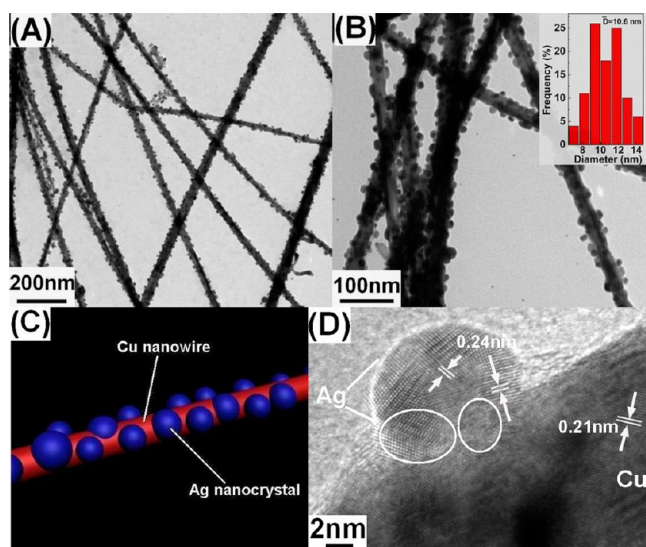

Figure 2. (A) Low- and (B) high-magnification TEM images of the octopus-tentacle-like Cu NW-Ag NCs heterostructures. (C) The schematic diagram of an individual heterostructure. (D) HRTEM image of the heterostructures. The two white circles show the dislocation or stacking fault areas.

TEM image (Figure 2A), we can see many small black dots decorated on each NW. In contrast to the initial Cu NWs (see Figure S1 in the Supporting Information), the observed black dots can be ascribed to Ag NCs, revealing that Ag NCs have been effectively grown on Cu NWs "seeds". Due to the deposition of Ag NCs, the originally smooth surfaces of Cu NWs become very rough, forming many protuberances and

letting the whole nanostructure look like the tentacle of an octopus. In high magnification TEM image (Figure 2B), many junctions can be observed between Cu NW and Ag NCs, confirming the formation of octopus-tentacle-like heterostructures. On each Cu NW-Ag NCs heterostructure, the distribution of Ag NCs on Cu NW is relatively uniform. By statistical analysis (inset of Figure 2B), the average size of formed Ag NCs is about 10.6 nm. Figure 2C gives the schematic diagram of an individual Cu NW-Ag NCs heterostructure. Corresponding HRTEM image (Figure 2D) reveals that the Ag NC is partially embedded into the surface of Cu NW. Also, some dislocations or stacking faults along the junction of Cu NW and Ag NCs can be observed, which are indicated by the white circles. To see clearly, the magnified image of Figure 2D is shown in Figure S2 in the Supporting Information. For Ag NC section, clear lattice fringes are observed and the lattice spacing is about 2.40 Å, corresponding to the (111) plane of fcc phase Ag. As for Cu NW section, the obvious lattice fringes are also seen. Related lattice spacing is about 2.10 Å, which can be indexed to (111) plane of fcc phase Cu. The HRTEM results confirm that the obtained product is Cu NW-Ag NCs heterostructures, not Cu−Ag alloy, which is consistent with XRD analysis. The EDS mapping analysis (see Figure S3 in the Supporting Information) further confirms the formation of heterostructures based on the distribution of Cu (interior of the nanowire) and Ag (exterior of the nanowire) elements.

To get some insight on the growth mechanism of Cu NW-Ag NCs heterostructures, we performed a series of control experiments. We find that the OA and DDA have a great impact on synthesis of the heterostructures. If only single OA is used as a surfactant and other conditions are kept constant, the Cu NW-Ag NCs heterostructures cannot be formed (Figure 3A) because the displacement reaction between Cu NWs and
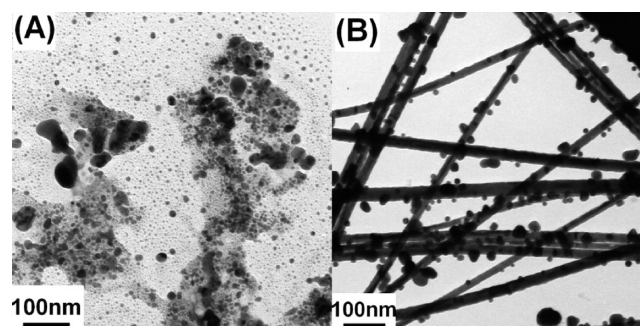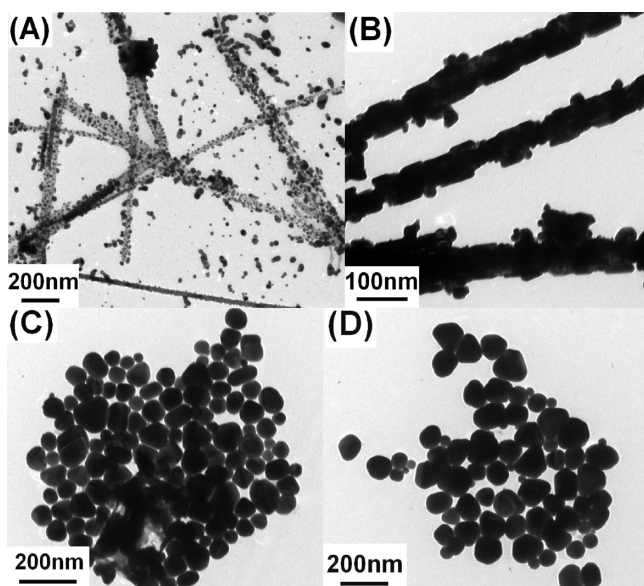

Figure 3. TEM images of the control samples obtained by using Cu NWs as "seeds" and adding $AgNO_3$ solution at 80 °C under different growth environments. (A) Only in the presence of oleic acid. (B) Only in the presence of dodecylamine.

Ag precursors occupies the dominant role. It leads the Cu NWs to be depleted under this case. When sole DDA is used as a surfactant, desired heterostructures can be obtained (Figure 3B), but the size and density of deposited Ag NCs are larger and lower than that under typical conditions, respectively. These results indicate that the galvanic displacement can be effectively inhibited in the presence of DDA, which is an efficient reductant. For controlling the size and density of formed Ag NCs, the optimal surfactant is the combination of DDA and OA. In addition, the reaction temperature also plays an important role for formation of Cu NW-Ag NCs

6656

dx.doi.org/10.1021/am301814y | ACS Appl. Mater. Interfaces 2012, 4, 6654−6660

heterostructures. Though the heterostructures can be obtained at 60 °C, some "free" Ag NCs are also observed (Figure 4A).


Figure 4. TEM images of the control samples obtained by using the equivalent Cu NWs as "seeds" and adding AgNO$_3$ solution at (A) 60, (B) 100, (C) 150, and (D) 200 °C, respectively.

Only at 80 °C (typical condition), high-quality Cu NW-Ag NCs heterostructures can be formed. In this case, the reduction rate of Ag precursors and diffusion rate of formed Ag nanoclusters may match, so the Ag NCs can grow well on Cu NW surface and no "free" Ag NCs exist. If the reaction temperature is raised to 100 °C, the Cu NWs are partially destroyed and their surfaces are covered with a layer of noncontinuous Ag film along with small amount of Ag "nanoislands" (Figure 4B). Further increasing the temperature to 150 °C (Figure 4C) and 200 °C (Figure 4D), Cu NWs completely disappear and only polyhedral nanoparticles generate, revealing that the galvanic reaction dominates when the temperature exceeds 100 °C. Corresponding EDS and XRD results (see Figure S4 in the Supporting Information) exhibit that the obtained products under those two conditions are pure Ag. Also, under the optimal surfactant and reaction temperature, the amount of Ag precursors is found to affect the deposition rate and status of Ag NCs on Cu NW surface. As the amount of Ag precursors is lower than that of typical condition (0.2 mmol), the noncontinuous Ag film overlayer can be clearly seen on each Cu NW. And only a few Ag NC islands are extrusive from the surface of Cu NW (see Figure S5A-B in the Supporting Information). While the amount of Ag precursors is higher than 0.2 mmol (see Figure S5C in the Supporting Information), some octopus-tentacle-like heterostructures with a high density of Ag NCs layers are formed. Except for these structures, there are many "free" Ag NCs resulting from homogeneous nucleation in solution. Those results demonstrate that control of growth environment and dynamic factors is vital for obtaining high-quality Cu NW-Ag NC heterostructures.

Usually, two main kinds of growth mechanisms are used to explain the formation of metal heterostructures. One is surface segregation of nanoalloy.[13,61] The other is heterogeneous nucleation and growth.[62] The former can be excluded because

the reaction temperature is too low (only 80 °C) to form Cu—Ag alloy. Thus, the formation of Cu NW-Ag NC heterostructures in our work should follow the latter mechanism. According to heterogeneous nucleation and growth theory, three primary growth modes are widely used to elucidate epitaxial growth of a desired substance on single-crystal surface in gas phase or vacuum system: (i) the layered growth (Frank—van der Merwe (F—M) mode); (ii) the island growth (Volmer—Weber (V—W) mode); (iii) the "layer-plus-island" growth (Stranski—Krastanow (S—K) mode).[63] Scheme 1 shows

Scheme 1. schematic diagram of three kinds of modes (cross-section views) for thin-film growth including (a) Frank-van der Merwe (F-M) mode, (b) Volmer-Weber (V—W) mode and (c) Stranski-Krastanow (S—K) mode. Each mode is shown for several different amounts of surface coverage θ. The abbreviation of ML stands for "monolayer"
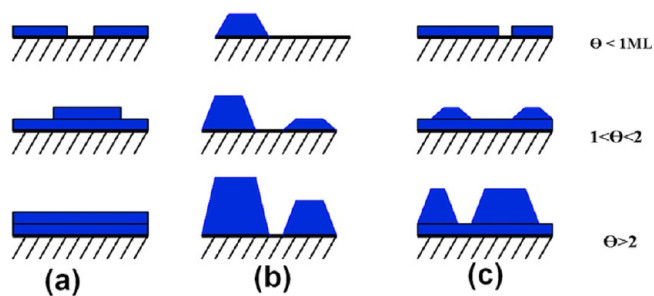
those three main growth modes for various surface coverage. The physical constants of the adatoms and substrate, such as electronegativity, metal bonding energy, and lattice match degree, are considered to be the key factors for determining the growth mode.[62,63] However, for growth of desired metal NCs on nanoscaled metal substrate in liquid phase, the case becomes complicate because of the existence of second metal ions, anions, reducing and capping reagents. So, besides the physical constants, the thermodynamic and kinetic factors as well as the synergistic effect of all factors should be considered to judge the growth mode. Table S1 in the Supporting Information summarizes the physical constants of Cu and Ag. Only considering from electronegativity, the galvanic displacement reaction takes place that is disadvantageous to epitaxial layer growth (F—M mode). In our experiments, by introducing DDA and controlling reaction temperature, the galvanic reaction can be effectively inhibited, which is helpful for Ag NCs to wet Cu NW surface and facilitates occurrence of F—M growth mode.[62] Additionally, the bonding energy of Ag—Ag and Ag—Cu also meets the rule for F—M growth mode.[62] However, no obvious concentric cablelike nanostructures are obtained in the final product, implying that pure F—M growth mode is difficult to occur in current system. This can be attributed to large lattice mismatch between Ag and Cu (~13%), leading to generate large strain at Cu—Ag interface. Although large strain can provide the driving force for formation of islands, the growth of Ag NCs on Cu NWs in our experiments cannot be simply assigned to pure V—W mode due to the bonding energy of Ag—Ag slightly smaller than that of Ag—Cu, which does not well meet the criterion for V—W mode.[63] On the basis of the above analysis, the growth mode of Ag NCs on Cu NW should conform to S—K mode. According to S—K mode,[63,64] the following two steps should occur: initially, an Ag film up to several monolayers thick grows in a layer-by-layer fashion on
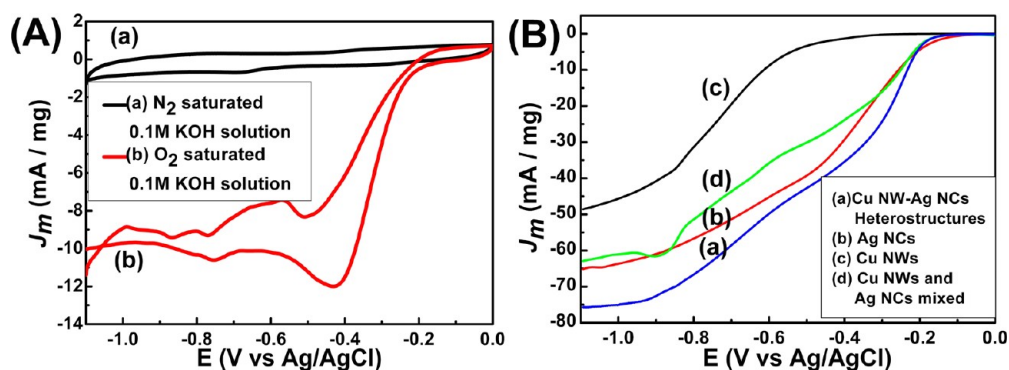
Figure 5. (A) CVs of Cu NW-Ag NCs heterostructures supported on glassy carbon substrate in (a) N_2 or (b) O_2 saturated 0.1 M KOH solution. Scan rate, 50 mV s^{-1}. (B) Rotating disk voltammograms obtained on thes (a) Cu NW-Ag NCs heterostructure, (b) pure Ag NCs, (c) pure Cu NWs, and (d) mechanically mixed Cu NWs and Ag NCs in 0.1 M KOH solution saturated with O_2 (1600 rpm; scan rate, 5 mV s^{-1}). The current density is expressed with respect to the mass of Ag plus Cu.

Cu NW surface. Beyond a critical layer thickness, the Ag film avalanches and coalescences to form small Ag NCs "islands". In the present work, many Ag NCs islands are clearly observed on Cu NW surface but Ag film overlayer is difficult to be seen, indicating the critical Ag film layer under this case is very thin. Besides the large lattice misfit between Ag and Cu,[65] the high chemical potential of Ag precursors in liquid phase may be another origin for presence of thin Ag film overlayer. The dislocations or stacking faults formed at the interfaces of Cu NW and Ag NC islands, which are confirmed by HRTEM analysis (Figure 2D or Figure S2 in the Supporting Infomration), can promote the release of accumulated lattice strain.[66] The influence of chemical potential of precursor solution on critical Ag film thickness can be further proved from control experiments. By decreasing the amount of Ag precursors, the thick Ag film overlayer and extrusive Ag NC islands are observed (see Figure S5A-B in the Supporting Information), exhibiting obvious features for S−K growth mode.

To verify the feasibility and versatility of our method, we also extend the synthetic strategy to prepare other binary metal heterostructures whose components have large lattice mismatch, such as the combination of Cu−Au (their lattice mismatch is about 12.8%) and Cu−Pd (their lattice mismatch is about 7.6%). The experimental results demonstrate that octopus-tentacle-like Cu NW-Au NCs and Cu NW-Pd NCs heterostructures can be obtained by using Cu NWs as "seeds" and controlling the growth environment and dynamic process of Au and Pd NCs. Corresponding TEM images are shown in Figure S6 in the Supporting Information.

The electrocatalytic performance of the octopus-tentacle-like Cu NW-Ag NCs heterostructures are evaluated with electrochemical measurements by depositing the heterostructures on a glassy carbon electrode. Figure 5A shows the cyclic voltammograms (CVs) of the Cu NW-Ag NCs heterostructures in 0.1 M KOH saturated with either N_2 or O_2 at a scan rate of 50 mV s^{-1}. Compared to the featureless CV profile in N_2-saturated electrolyte, a strong reduction current peak can be seen with the electrolyte saturated with O_2, revealing the high electrocatalytic activity of the Cu NW-Ag NCs heterostructures toward ORR. To get some insight on the catalytic behaviors, the ORR at Cu NW-Ag NCs heterostructures, pure Cu NWs, and pure Ag NCs catalysts with the same mass loading are further investigated with rotating disk voltammetry. The corresponding polarization curves are shown in Figure 5B.

From Figure 5B, we can see that the onset reduction potentials of O_2 on those three catalysts are −0.14, −0.42, and −0.12 V, respectively. Compared with that of pure Cu NWs, the onset reduction potential of O_2 on Cu NW-Ag NCs heterostructures is greatly positive shift about 0.28 V. Compared to pure Ag NCs (∼10 nm, see Figure S7 in the Supporting Information), only a slight negative shift of O_2 onset reduction potential is observed on Cu NW-Ag NCs heterostructure catalyst. As is known to all, Ag is one of the noble metals and usually used as a catalyst for ORR reaction in alkaline fuel cells.[67] In our work, by partially substitution of Ag NCs with cheap Cu NW and fabrication of Cu NW-Ag NCs heterostructures, the onset reduction potential for O_2 has no obvious change, implying that the obtained Cu NW-Ag NCs heterostructures can replace pure Ag NCs to catalyze ORR. Moreover, the mass current density (J_m) for ORR on Cu NW-Ag NCs heterostructures catalyst is much higher than that on pure Cu NWs and pure Ag NCs catalysts at the potential ranging from −0.2 V to −1.1 V. These results demonstrate that the Cu NW-Ag NCs heterostructures possess enhanced electrocatalytic performance for ORR compared with that of their individual component. The obvious enhanced catalytic performance on Cu NW-Ag NCs heterostructures can be attributed to the presence of multiple junctions and strong synergistic effect of their constituents. For confirming the junction and synergistic effect, a control experiment by using mechanically mixed Cu NWs and Ag NCs samples with the same mass loading as a catalyst is carried out. On mechanically mixed dual components, the O_2 onset reduction potential is close to that of Cu NW-Ag NCs heterostructures, but the J_m value is much smaller than that on heterostructures and pure Ag NCs catalysts. That is to say, the catalytic performance of the heterostructures is much better than that of mechanically mixed dual components. Further evidence for synergistic effect of the binary components in heterostructures comes from their electronic spectra (see Figure S8 in the Supporting Information). Despite the lower catalytic performance compared to traditional Pt-based and some Pt-free catalysts,[68] the present octopus-tentacle-like Cu NW-Ag NCs heterostructures actually exhibit catalytic activity comparable with or even better than that of other non-Pt materials, such as small Ag nanoparticles,[69] icosahedral Ag or Au nanostructures,[70] Cu_3N nanocubes,[71] commercial Pd/C catalyst,[71] and N-doped graphene quantum dots.[72] Moreover, the stability measurements demonstrate that there is a little decrease in current density after continuous sweeping for 2000

cycles in O_2-saturated 0.1 M KOH (see Figure S9 in the Supporting Information), indicating a slight loss of catalytic activity for Cu NW-Ag NCs heterostructural catalyst. Although its stability needs to be further improved compared with that of Pt-based catalysts, such novel non-Pt heterostructural electrocatalyst shows great promise for applying in alkaline fuel cells with the advantage of low cost and high mass current density.

4. CONCLUSION

In conclusion, the octopus-tentacle-like Cu NW-Ag NCs heterostructures have been synthesized in solution phase through heterogeneous nucleation and growth of Ag NCs on presynthesized Cu NW "seeds". The EDS and XRD results show that the components of the obtained heterostructures are Cu and Ag with face-centered cubic phase structure. TEM analysis reveals that the distribution of Ag NCs on presynthesized Cu NWs is relatively uniform and the average size of formed Ag NCs is about 10.6 nm. Corresponding HRTEM analysis confirms that the Ag NCs are well-crystallined and there are some dislocations or defects between the interface of Ag NCs and Cu NWs. A series of control experiments demonstrate that control of growth environment and dynamic process is vital for formation of the octopus-tentacle-like Cu NW-Ag NCs heterostructures. By introducing DDA and controlling reaction temperature, the galvanic displace reaction between Ag precursors and Cu NWs can be effectively inhibited, facilitating the formed Ag nanoclusters to wet Cu NWs surfaces. The large lattice misfit between Ag and Cu provides the driving force for switching the growth of Ag NCs from F−M to V−W mode, leading the epitaxial growth means of Ag NCs on Cu NW to abide by S−K mode. Electrocatalytic experiments demonstrate that the obtained Cu NW-Ag NCs heterostructures exhibit greatly enhanced electrocatalytic performance for ORR in alkaline media compared with those of pure Ag NCs, Cu NWs, and mechanically mixed dual components as well as recently reported some non-Pt catalysts. The enhanced electrocatalytic acitivity of the heterostructures is attributed to presence of multiple junctions and strong synergistic effect of their constituents. Furthermore, our method can be extended to fabricate Cu NW-Au NCs and Cu NW-Pd NCs heterostructures. This work not only provides an efficient avenue for synthesizing metal heterostructures with large lattice misfit (>5%) but also paves the way to design non-Pt nanocatalysts for applying in clean energy source and other advanced technological fields.

ASSOCIATED CONTENT

Ⓢ Supporting Information

Additional experimental details for synthesis of Cu NWs "seeds" and pure Ag NCs control catalyst, structural characterization of Cu NWs (Figure S1), magnified HRTEM image (Figure S2), and EDS mapping characterization of Cu NW-Ag NCs heterostructures (Figure S3), some control experiments results (Figure S4−S7), physical constants of Cu and Ag (Table S1), electrical spectra of the heterostructures (Figure S8), and electrochemical stability measurement results for the heterostructures (Figure S9). This material is available free of charge via the Internet at http://pubs.acs.org/.

AUTHOR INFORMATION

Corresponding Author
*Phone: +86-25-85891936. Fax: +86-25-85891936. E-mail: baojianchun@njnu.edu.cn (J.B.); daizhihuii@njnu.edu.cn (Z.D.).

Notes
The authors declare no competing financial interest.

ACKNOWLEDGMENTS

REFERENCES

(1) Major, K. J.; De, C.; Obare, S. O. *Plasmonics* **2009**, *4*, 61−78.
(2) Wang, L.; Clavero, C.; Huba, Z.; Carroll, K. J.; Carpenter, E. E.; Gu, D. F.; Lukaszew, R. A. *Nano Lett.* **2011**, *11*, 1237−1240.
(3) Alayoglu, S.; Nilekar, A. U.; Mavrikakis, M.; Eichhorn, B. *Nat. Mater.* **2008**, *7*, 333−338.
(4) Mazumber, V.; Chi, M. F.; More, K. L.; Sun, S. H. *J. Am. Chem. Soc.* **2010**, *132*, 7848−7849.
(5) Tao, F.; Grass, M. E.; Zhang, Y. W.; Butcher, D. R.; Aksoy, F.; Aloni, S.; Altoe, V.; Alayoglu, S.; Renzas, J. R.; Tsung, C. K.; Zhu, Z. W.; Liu, Z.; Salmeron, M.; Somorjai, G. A. *J. Am. Chem. Soc.* **2010**, *132*, 8697−8703.
(6) Wang, F.; Li, C. H.; Sun, L. D.; Wu, H. S.; Ming, T. A.; Wang, J. F.; Yu, J. C.; Yan, C. H. *J. Am. Chem. Soc.* **2011**, *133*, 1106−1111.
(7) Son, S. U.; Jang, Y.; Park, J.; Na, H. B.; Park, H. M.; Yun, H. J.; Lee, J.; Hyeon, T. *J. Am. Chem. Soc.* **2004**, *126*, 5026−5027.
(8) Ferrer, D.; Torres-Castro, A.; Gao, X.; Sepulveda-Guzman, S.; Ortiz-Mendez, U.; Jose-Yacaman, M. *Nano Lett.* **2007**, *7*, 1701−1705.
(9) Kyriakou, G.; Boucher, M. B.; Jewell, A. D.; Lewis, E. A.; Lawton, T. J.; Baber, A. E.; Tierney, H. L.; Flytzani-Stephanopoulos, M.; Sykes, E. C. H. *Science* **2012**, *335*, 1209−1212.
(10) Gao, W.; Sattayasamitsathit, S.; Manesh, K. M.; Weihs, D.; Wang, J. *J. Am. Chem. Soc.* **2010**, *132*, 14403−14405.
(11) Lee, J. H.; Wu, J. H.; Liu, H. L.; Cho, J. U.; Cho, M. K.; An, B. H.; Min, J. H.; Noh, S. J.; Kim, Y. K. *Angew. Chem., Int. Ed.* **2007**, *46*, 3663−3667.
(12) Liang, H. P.; Guo, Y. G.; Hu, J. S.; Zhu, C. F.; Wan, L. J.; Bai, C. L. *Inorg. Chem.* **2005**, *44*, 3013−3015.
(13) Mayrhofer, K. J. J.; Juhart, V.; Hartl, K.; Hanzlik, M.; Arenz, M. *Angew. Chem., Int. Ed.* **2009**, *48*, 3529−3531.
(14) Sanedrin, R. G.; Georganopoulou, D. G.; Park, S.; Mirkin, C. A. *Adv. Mater.* **2005**, *17*, 1027−1031.
(15) Habas, S. E.; Lee, H.; Radmilovic, V.; Somorjai, G. A.; Yang, P. D. *Nat. Mater.* **2007**, *6*, 692−697.
(16) Lim, B.; Jiang, M. J.; Camargo, P. H. C.; Cho, E. C.; Tao, J.; Lu, X. M.; Zhu, Y. M.; Xia, Y. N. *Science* **2009**, *324*, 1302−1305.
(17) Salem, A. K.; Chao, J.; Leong, K. W.; Searson, P. C. *Adv. Mater.* **2004**, *16*, 268−271.
(18) Wang, D. S.; Li, Y. D. *J. Am. Chem. Soc.* **2010**, *132*, 6280−6281.
(19) Yamauchi, T.; Tsukahara, Y.; Yamada, K.; Sakata, T.; Wada, Y. *Chem. Mater.* **2011**, *23*, 75−84.
(20) Pingali, K. C.; Deng, S. G.; Rockstraw, D. A. *Power Technol.* **2008**, *183*, 282−289.

(21) Lim, B.; Kobayashi, H.; Yu, T.; Wang, J. G.; Kim, M. J.; Li, Z. Y.; Rycenga, M.; Xia, Y. N. *J. Am. Chem. Soc.* **2010**, *132*, 2506−2507.

(22) Zhang, H.; Jin, M. S.; Wang, J. G.; Kim, M. J.; Yang, D. R.; Xia, Y. N. *J. Am . Chem. Soc.* **2011**, *133*, 10422−10425.

(23) Zhang, J. T.; Tang, Y.; Weng, L.; Ouyang, M. *Nano Lett.* **2009**, *9*, 4061−4065.

(24) Huang, X. Q.; Tang, S. H.; Liu, B. J.; Ren, B.; Zheng, N. F. *Adv. Mater.* **2011**, *23*, 3420−3425.

(25) Lu, C. L.; Prasad, K. S.; Wu, H. L.; Ho, J. A.; Huang, M. H. *J. Am. Chem. Soc.* **2010**, *132*, 14546−14553.

(26) Yu, Y.; Zhang, Q. B.; Liu, B.; Lee, J. Y. *J. Am. Chem. Soc.* **2010**, *132*, 18258−18265.

(27) Wang, C.; Tian, W. D.; Ding, Y.; Ma, Y. Q.; Wang, Z. L.; Markovic, N. M.; Stamenkovic, V. R.; Daimon, H.; Sun, S. H. *J. Am. Chem. Soc.* **2010**, *132*, 6524−6529.

(28) Seo, D.; Yoo, C. I.; Jung, J.; Song, H. *J. Am. Chem. Soc.* **2008**, *130*, 2940−2941.

(29) Tan, Y. M.; Fan, J. M.; Chen, G. X.; Zheng, N. F.; Xie, Q. *J. Chem. Commun.* **2011**, *47*, 11624−11626.

(30) Guo, S. J.; Dong, S. J.; Wang, E. K. *Chem. Commun.* **2010**, *46*, 1869−1871.

(31) Gasteiger, H. A.; Markovic, N. M. *Science* **2009**, *324*, 48−49.

(32) Peng, Z. M.; Yang, H. *Nano Today* **2009**, *4*, 143−164.

(33) Sun, S. H.; Jaouen, F.; Dodelet, J. P. *Adv. Mater.* **2008**, *20*, 3900−3904.

(34) Lee, E. P.; Peng, Z. M.; Chen, W.; Chen, S. W.; Yang, H.; Xia, Y. N. *ACS Nano* **2008**, *2*, 2167−2173.

(35) Zhou, H. J.; Zhou, W. P.; Adzic, R. R.; Wong, S. S. *J. Phys. Chem. C* **2009**, *113*, 5460−5466.

(36) Liang, H. W.; Cao, X.; Zhou, F.; Cui, C. H.; Zhang, W. J.; Yu, S. H. *Adv. Mater.* **2011**, *23*, 1467−1471.

(37) Ma, X. M.; Meng, H.; Cai, M.; Shen, P. K. *J. Am. Chem. Soc.* **2012**, *134*, 1954−1957.

(38) Wu, Z. X.; Lv, Y. Y.; Xia, Y. Y.; Webley, P. A.; Zhao, D. Y. *J. Am. Chem. Soc.* **2012**, *134*, 2236−2245.

(39) Stamenkovic, V. R.; Fowler, B.; Mun, B. S.; Wang, G. F.; Ross, P. N.; Lucas, C. A.; Markovic, N. M. *Science* **2007**, *315*, 493−497.

(40) Snyder, J.; Fujita, T.; Chen, M. W.; Erlebacher, J. *Nat. Mater.* **2010**, *9*, 904−907.

(41) Wu, J. B.; Zhang, J. L.; Peng, Z. M.; Yang, S. C.; Wagner, F. T.; Yang, H. *J. Am. Chem. Soc.* **2010**, *132*, 4984−4985.

(42) Kim, J.; Lee, Y.; Sun, S. H. *J. Am. Chem. Soc.* **2010**, *132*, 4996−4997.

(43) Guo, S. J.; Sun, S. H. *J. Am. Chem. Soc.* **2012**, *134*, 2492−2495.

(44) Shao, M.; Sasaki, K.; Adzic, R. R. *J. Am. Chem. Soc.* **2006**, *128*, 3526−3527.

(45) Suo, Y.; Zhuang, L.; Lu, J. *Angew. Chem., Int. Ed.* **2007**, *46*, 2862−2864.

(46) Xu, C. X.; Zhang, Y.; Wang, L. Q.; Xu, L. Q.; Bian, X. F.; Ma, H. Y.; Ding, Y. *Chem. Mater.* **2009**, *21*, 3110−3116.

(47) Lee, K. R.; Jung, Y.; Woo, S. I. *ACS Comb. Sci.* **2012**, *14*, 10−16.

(48) Gao, M. R.; Jiang, J.; Yu, S. H. *Small* **2012**, *8*, 13−27.

(49) Gong, K. P.; Du, F.; Xia, Z. H.; Durstock, M.; Dai, L. M. *Science* **2009**, *323*, 760−764.

(50) Liang, Y. Y.; Li, Y. G.; Wang, H. L.; Zhou, J. G.; Wang, J.; Regier, T.; Dai, H. *J. Nat. Mater.* **2011**, *10*, 780−786.

(51) Cheng, F. Y.; Shen, J. A.; Peng, B.; Pan, Y. D.; Tao, Z. L.; Chen, J. *Nat. Chem.* **2011**, *3*, 79−84.

(52) Wiberg, G. K. H.; Mayrhofer, K. J. J.; Arenz, M. *Fuel Cells* **2010**, *4*, 575−581.

(53) Guo, J. S.; Hsu, A.; Chu, D.; Chen, R. R. *J. Phys. Chem. C* **2010**, *114*, 4324−4330.

(54) Fernandez, J. L.; Walsh, D. A.; Bard, A. J. *J. Am. Chem. Soc.* **2005**, *127*, 357−365.

(55) Lima, F. H. B.; de Castro, J. F. R.; Ticianelli, E. A. *J. Power Sources* **2006**, *161*, 806−812.

(56) Schwamborn, S.; Stoica, L.; Schuhmann, W. *ChemPhysChem* **2011**, *12*, 1741−1746.

(57) Lee, C.-L.; Chiou, H.-P.; Syu, C.-M.; Liu, C.-R.; Yang, C.-C.; Syu, C.-C. *Int. J. Hydrogen Energ.* **2011**, *36*, 12706−12714.

(58) Feng, Y.-Y.; Zhang, G.-R.; Ma, J.-H.; Liu, G.; Xu, B.-Q. *Phys. Chem. Chem. Phys.* **2011**, *13*, 3863−3872.

(59) Slana, D. A.; Hardin, W. G.; Johnston, K. P.; Stevenson, K. J. *J. Am. Chem. Soc.* **2012**, *134*, 9812−9819.

(60) Ye, E. Y.; Zhang, S. -Y.; Liu, S. H.; Han, M.-Y. *Chem.—Eur. J.* **2011**, *17*, 3074−3077.

(61) Wang, D. L.; Xin, H. L.; Yu, Y. C.; Wang, H. S.; Rus, E.; Muller, D. A.; Abruña, H. D. *J. Am. Chem. Soc.* **2010**, *132*, 17664−17666.

(62) Fan, F. R.; Liu, D. Y.; Wu, Y. F.; Duan, S.; Xie, Z. X.; Jiang, Z. Y.; Tian, Z. Q. *J. Am. Chem. Soc.* **2008**, *130*, 6949−6951.

(63) Markov, I. V. In *Crystal Growth for Beginners: Fundamentals of Nucleation, Crystal Growth, and Epitaxy*, 2nd ed.; MarKov, I. V., Ed.; World Scientific Publishing: Singapore, 2003; Chapter 4, pp 353−466.

(64) Chiu, C.-H.; Huang, Z.; Poh, C. T. *Phys. Rev. Lett.* **2004**, *93*, 36105−1−36105−4.

(65) Matthews, J. W. In *Epitaxial Growth*, 1st ed.; Matthews, J. W., Ed.; Academic Press: New York, 1975; Vol. 2, pp 381−393.

(66) Shklyaev, O. E.; Beck, M. J.; Asta, M.; Miksis, M. J.; Voorhees, P. W. *Phys. Rev. Lett.* **2005**, *94*, 176102−1−176102−4.

(67) Yi, B. L. In *The Principle, Technology and Application of Fuel Cells*; 1st ed.; Yi, B. L., Ed.; Chemical Industry Press: Beijing, 2003; Chap. 1, P 30−31.

(68) Winther-Jensen, B.; Winther-Jensen, O.; Forsyth, M.; MacFarlane, D. R. *Science* **2008**, *321*, 671−674.

(69) Lu, Y. Z.; Chen, W. *J. Power Sources* **2012**, *197*, 107−110.

(70) Kuai, L.; Geng, B. Y.; Wang, S. Z.; Zhao, Y. Y.; Luo, Y. C.; Jiang, H. *Chem.—Eur. J.* **2011**, *17*, 3482−3489.

(71) Wu, H. B.; Chen, W. *J. Am. Chem. Soc.* **2011**, *133*, 15236−15239.

(72) Li, Y.; Zhao, Y.; Cheng, H. H.; Hu, Y.; Shi, G. Q.; Dai, L. M.; Qu, L. T. *J. Am. Chem. Soc.* **2012**, *134*, 15−18.

6660

dx.doi.org/10.1021/am301814y | *ACS Appl. Mater. Interfaces* 2012, 4, 6654−6660